High Sensitivity CW-Cavity Ring Down Spectroscopy of 12CO2 near 1.35 μm (II): New observations and Line intensities modeling

K.F. Song, Samir Kassi, S.A. Tashkun, V.I. Perevalov, Alain Campargue

High Sensitivity *CW*-Cavity Ring Down Spectroscopy of five $^{13}CO_2$ isotopologues of carbon dioxide in the 1.26-1.44 μm region (I): Line positions

A. Campargue[*1], K. F. Song[*], N. Mouton[*], V.I. Perevalov[&] and S. Kassi[*]

[*]*Laboratoire de Spectrométrie Physique (associated with CNRS, UMR 5588), Université Joseph Fourier de Grenoble, B.P. 87, 38402 Saint-Martin-d'Hères Cedex, France*
[&]*Laboratory of Theoretical Spectroscopy, Institute of Atmospheric Optics, SB, Russian Academy of Science, 1, Akademicheckii av., 634055, Tomsk, Russia*

12/11/2009

Key words: Carbon dioxide, CO2, Cavity Ring Down Spectroscopy, effective hamiltonian, HITRAN, HITEMP, CDSD, Venus, isotopologue

[1] Corresponding author: Alain. Campargue@ujf-grenoble.fr

Abstract

The absorption spectrum of highly enriched ^{13}C carbon dioxide has been investigated by CW-Cavity Ring Down Spectroscopy with a setup based on fibered distributed feedback (DFB) laser diodes. By using a series of 30 DFB lasers, the CO_2 spectrum was recorded in the 7029-7917 cm^{-1} region with a typical sensitivity of 3×10^{-10} cm^{-1}. The uncertainty on the determined line positions is on the order of 8×10^{-4} cm^{-1}. More than 3800 transitions with intensities as low as 1×10^{-29} cm/molecule were detected and assigned to the $^{13}C^{16}O_2$, $^{16}O^{13}C^{17}O$, $^{16}O^{13}C^{18}O$, $^{17}O^{13}C^{18}O$ and $^{13}C^{18}O_2$ isotopologues. For comparison, only 104 line positions of $^{13}C^{16}O_2$ were previously reported in the literature in the considered region. The band by band analysis has led to the determination of the rovibrational parameters of a total of 83 bands including 56 bands of the $^{13}C^{16}O_2$ species. The measured line positions of $^{13}C^{16}O_2$ and $^{16}O^{13}C^{18}O$ were found in good agreement with the predictions of the respective effective Hamiltonian (EH) models but the agreement degrades for the minor isotopologues. Several cases of resonance interactions were found and discussed. In the 20033-10002 band of $^{13}C^{16}O_2$, an anharmonic resonance interaction leads to deviations on the order of 0.05 cm^{-1} compared to the EH predictions. The existence of interpolyad interactions affecting the non symmetric isotopologues of carbon dioxide is confirmed by the observation of two occurrences in $^{16}O^{13}C^{17}O$ and $^{16}O^{13}C^{18}O$. The obtained results improve significantly the knowledge of the spectroscopy of the ^{13}C isotopologues of carbon dioxide. They will be valuable to refine the sets of effective Hamiltonian parameters used to generate the CDSD database.

I. INTRODUCTION

The present work is devoted to the highly sensitive absorption spectroscopy of ^{13}C isotopologues of carbon dioxide. The high resolution spectra of such minor isotopologues are very important in the studies of Venus and Mars atmospheres for which this gas is a principal constituent. The ground and satellite based infrared sensors used for these purposes work in the transparency windows of these atmospheres. Due to isotopic shifts and due to the changing of the symmetry under isotopic substitution, the contribution of the minor isotopologues to the absorption in the transparency windows may largely exceed that of the principal isotopologue in spite of their small relative concentrations. Considering the large optical thickness in the atmospheres of these planets, the absorption of the minor isotopologues must then be accurately characterized. In addition, the knowledge of the concentrations of the minor isotopologues themselves is also very important for the atmospheric physics of these planets. For more details we refer readers to the recent publications [1-4].

This contribution is part of the series of our publications devoted to the investigations of the absorption spectrum of carbon dioxide by high sensitivity CW-Cavity Ring Down Spectroscopy (CW-CRDS) in the spectral region accessible with distributed feedback (DFB) laser diodes. This technique is a very powerful tool for the study of high resolution spectra of minor isotopologues. A first series of reports were devoted to natural carbon dioxide and ^{13}C enriched isotopologues in the 5851-7045 cm^{-1} region (1.71-1.42 μm) [5-12]. The achieved sensitivity allows detecting numerous new transitions with intensity down to 10^{-29} cm/molecule. In this 5851-7045 cm^{-1} region, the recent HITRAN2008 database [13] has adopted the CRDS line positions for the transitions below the detection limit (about 10^{-26} cm/molecule) of the measurements performed at Jet Propulsion Laboratory (JPL) by Fourier Transform Spectroscopy (FTS) [14-21]. Together with all the measurements available in the literature, these FTS and CRDS experimental values were used as input data in order to refine the parameters of the global effective Hamiltonian (EH) model and improve the theoretical Carbon Dioxide Spectroscopic Databank (CDSD) [22]. For the weak lines not present in the CRDS and JPL datasets and blended lines unobserved by CRDS due to overlapping with stronger lines, the HITRAN2008 line list [13] was completed with the CDSD line parameters down to an intensity cut off of 4×10^{-30} cm/molecule.

We have developed a second DFB laser CW-CRDS spectrometer dedicated to the 7000-7920 cm^{-1} range. It was applied for the first time to carbon dioxide in natural abundance [23,24]. A global list of 2881 lines was constructed for the four isotopologues contributing to the CRDS spectrum in the 7123-7917 cm^{-1} region. These CW-CRDS observations represented a significant improvement in terms of accuracy and sensitivity compared to Venus spectra (about 470 lines) [25] which were the main experimental source for line positions in the region. Some deviations between the observations and the CDSD calculations (used for HITRAN2008) were evidenced both for the line positions and line intensities. The measured line intensities allowed determining the ΔP=10 set of effective dipole parameters of $^{16}O^{12}C^{18}O$ and refining that of the ΔP=11 series of the principal isotopologue [24,26].

The present work is a very similar investigation devoted to the CW-CRDS spectrum of highly enriched ^{13}C carbon dioxide. The investigated spectral interval corresponds to a weak absorption region between the strong $3\nu_3$ band centered at 6780 cm^{-1} and the $\nu_1+3\nu_3$ dyad bands around 8000 cm^{-1}. Because the transitions are all weaker than 5×10^{-25} cm/molecule, in its 2004 version, the HITRAN database did not provide any $^{13}C^{16}O_2$ transition in our range. In its 2008 version, the HITRAN line list provided 1032 transitions which were all transferred from the theoretical Carbon Dioxide Spectroscopic Databank (CDSD). Previous observations relative to the ^{13}C isotopologues of carbon dioxide are very scarce: only 64 lines belonging to the 40012-00001 and 40013-00001 bands were identified in Venus spectra in the considered region [25]. This dataset was extended to 114 lines (belonging to the 40013-00001, 40012-00001, 11132-01101 bands) from FTS spectra recorded at USTC (Hefei) using a CO_2 sample with 99 % enrichment in ^{13}C and a 105 meter absorption path length [27]. The detection of 403 $^{13}CO_2$ lines in our CW-CRDS spectrum of carbon dioxide in natural isotopic abundance illustrates the higher sensitivity allowed by this technique. The line list provided as Supplementary Material attached to Ref. [23] includes these 403 transitions but the detailed analysis of the $^{13}CO_2$ bands was not reported as the present investigation performed with ^{13}C enriched sample provides a much more complete dataset. For instance, 2382 transitions of $^{13}C^{16}O_2$ and 1044 those of $^{16}O^{13}C^{18}O$ were identified in the present study.

After description of the experimental details (Section 2), the rovibrational assignment and the comparison with the EH predictions will be presented in Section 3. Section 4 will be devoted

to the band by band fit and to the analysis of a number of *intra*- and *inter*- polyad interactions which were identified.

II. EXPERIMENT

The fibered DFB laser CW-CRDS spectrometer developed for the 7000-7900 cm^{-1} region is essentially identical to the one used in our previous studies [5-12] dedicated to the 5900-7000 cm^{-1} range. The reader is referred to Refs. [7, 24, 28, 29] for the description of the experimental apparatus. The data acquisition has been updated compared to the first set up, leading to slightly better performances for both the sensitivity and wavenumber accuracy. The 7029-7917 cm^{-1} region was covered with the help of 30 fibered DFB lasers. The DFB typical tuning range is about 40 cm^{-1} by temperature tuning from -5°C to 60°C. The spectral coverage is complete except for a 3.5 cm^{-1} gap between 7897.2 and 7900.7 cm^{-1}. The stainless steel ringdown cell (l= 2 m, Φ= 10 mm) is fitted by a pair of super mirrors. Two sets of supermirrors were used. The first set used below 6610 cm^{-1}, leads to ringdown time varying smoothly from 50 to 70 μs according to the laser wavelength. The supermirrors used above 6610 cm^{-1} have a higher reflectivity (τ~ 150 μs) allowing for an increased sensitivity. About one hundred ringdown events were averaged for each spectral data point, and about 60 minutes were needed in order to complete a temperature scan of one DFB laser. The corresponding noise level on the spectrum baseline varied from 5×10^{-10} to 1×10^{-10} cm^{-1}, depending on the ringdown time. Fig. 1 illustrates the achieved sensitivity and dynamic range on the intensity scale in the region of the 40012-00001 band: absorption coefficients ranging from $\alpha \sim 4\times10^{-6}$ cm^{-1} down to the noise level at 3×10^{-10} cm^{-1} can be measured from the displayed spectrum.

The pressure (measured by a capacitance gauge) and the ringdown cell temperature were monitored during the spectrum recording. The pressure value was fixed to 13.3 hPa (10.0 Torr). The DFB linewidth is about one thousandth of the Doppler broadening leading to a mostly Gaussian line profile. The line centres were determined by using an interactive least squares multi-line fitting program assuming a line profile of Voigt type. The fitting procedure will be presented in more detail in a future contribution devoted to the line intensity analysis.

Each 40 cm^{-1} wide spectrum recorded with one DFB laser was calibrated independently on the basis of the wavelength values provided by the Michelson-type wavemeter (Burleigh WA-1650, 60 MHz resolution and 100 MHz accuracy). Considering that the speed of the DFB laser

frequency scan varies by about a factor 3 over the 7 tuning range a correction has to be applied to the wavemeter readings. The adopted procedure is detailed in Ref. [7]. The calibration was further refined by stretching the whole spectrum in order to match accurate positions of a few tens of reference lines observed in each spectrum. The HITRAN positions [13] of H_2O transitions present as an impurity in our sample were used for calibration. The typical uncertainty on the CO_2 line positions is estimated to be 8×10^{-4} cm^{-1} as it is confirmed by the band by band fit the spectroscopic parameters (see below) which leads to *rms* values which are generally better than 1×10^{-3} cm^{-1}.

III. ROVIBRATIONAL ASSIGNMENT

The main difficulties of the analysis arise from the superposition of the lines of seven isotopologues: $^{13}C^{16}O_2$, $^{16}O^{13}C^{18}O$, $^{16}O^{13}C^{17}O$, $^{17}O^{13}C^{18}O$, $^{13}C^{18}O_2$, $^{12}C^{16}O_2$ and $^{16}O^{12}C^{18}O$ (labelled hereafter 636, 638, 637, 738, 838, 626 and 628, respectively). Fig. 2 shows a 1.2 cm^{-1} wide section of spectrum were transitions of four ^{13}C isotopologues are observed. The overlapping with H_2O transitions (which are particularly strong below 7300 cm^{-1}) further complicated the analysis in the low frequency part of the spectrum.

The 626 and 628 transitions were easily identified by comparison with the CW-CRDS line list obtained for natural carbon dioxide [24]. The other transitions were assigned by comparison with the spectrum predicted with the respective EH models: Ref. [6] for 636, Ref. [8] for 637 and 638, Ref. [30] for 738 and Ref. [31] for 838. An additional difficulty of the assignment process was due to the fact that the EH predictions are of lower quality for the $^{13}CO_2$ isotopologues compared to those relative to the $^{12}CO_2$ species.

The EH models are polyad models. Each polyad is labelled by an integer $P= 2V_1+V_2+3V_3$ resulting from the approximate relations between the harmonic frequencies, $\omega_1 \approx 2\omega_2$ and $\omega_3 \approx 3\omega_2$. The vibrational basis states of a given polyad are coupled by anharmonic and Coriolis resonance interactions. Except for two ΔP=10 bands of the $^{16}O^{13}C^{18}O$ isotopologue at 7017 and 7125 cm^{-1}, all the bands in our region correspond to a ΔP=11 variation of the polyad quantum numbers. The 4001*i*-00001 (*i*=1-5) bands of the $4\nu_1+\nu_3$ pentad dominating the spectrum are accompanied by hot bands from *P*= 1-3 lower states. These hot bands provide valuable information about upper levels belonging to the *P*= 11-14 polyads which are lying largely above the studied range. For instance the 10042 state (*P*= 14) at 10172.78 cm^{-1} could be detected through a hot band from the 00011 state (*P*= 3) near 2283 cm^{-1}.

Finally 2382, 333, 1044, 52 and 30 transitions were assigned to the $^{13}C^{16}O_2$, $^{16}O^{13}C^{17}O$ and $^{16}O^{13}C^{18}O$, $^{13}C^{18}O_2$ and $^{17}O^{13}C^{18}O$ isotopologues, respectively. In the complete line list, provided as Supplementary Material, the experimental line positions are given for each line, together with the rovibrational assignments. An overview comparison of the assigned transitions is presented in Fig. 3 for the above three major ^{13}C isotopologues. Fig. 4 presents the corresponding (ν_{obs}-ν_{CDSD}) deviations. For the 636 isotopologue, the average and the root mean square (*rms*) values of the deviations are -6.3×10^{-4} and 6.5×10^{-3} cm^{-1}, respectively. The largest deviations correspond to the perturbed 20033-10002 band which will be discussed in Section 4. For the 638 isotopologue, the corresponding values are 4.8×10^{-3} and 8.9×10^{-3} cm^{-1}, respectively, the largest deviations being due to the local perturbation of the 40014-00001 band near 7221 cm^{-1}. As expected, the quality of the predictions degrades for the 637 minor isotopologue for which six bands were detected. The deviations of the band centres range between -0.9 and +0.4 cm^{-1} (see Fig. 4).

Overall, 56, 6 and 18 bands of the 636, 637 and 638 were identified. In addition, the 10031-00001 bands of the 738 and 838 isotopologues and the 10032-00001 band of the 838 isotopologue were detected in the high energy part of the spectrum. It leads to a total number of 83 bands, all of them, except four bands, being newly detected (see the statistics summarized in Table 1).

It should be emphasized that the 10031 and 10032 vibrational states of 838 and the 10031 vibrational state of 738 are the most excited states ever observed for these isotopologues.

IV. BAND-BY-BAND ANALYSIS

The usual expression of the vibration-rotational energy levels was used to fit the spectroscopic parameters to the observed wavenumbers:

$$F_v(J) = G_v + B_v J(J+1) - D_v J^2(J+1)^2 + H_v J^3(J+1)^3, \quad (1)$$

where G_v is the vibrational term value, B_v is the rotational constant, D_v and H_v are centrifugal distortion constants, J is the angular momentum quantum number.

In the case of hot bands involving *e* and *f* rotational levels, the *ee*, *ef*, *fe* and *ff* sub bands were considered independently. The lower state rotational constants were constrained to their literature values: $^{13}C^{16}O_2$ [16, 32], $^{16}O^{13}C^{18}O$ [16], $^{16}O^{13}C^{17}O$ [32], $^{13}C^{18}O_2$ [20] and $^{17}O^{13}C^{18}O$ [33]. The 10032-00001 band and the associated 11132-01101 hot band of $^{13}C^{16}O_2$ are centred

above the high energy limit of the investigated region and only *P* branch transitions could be measured. In order to enlarge the input data set and obtain reliable values of the spectroscopic parameters, the set of line positions measured by CRDS was completed by the line positions measured by FTS above 7917 cm^{-1} [6].

Tables 2-4 list the retrieved rovibrational parameter values for the bands of the 636, 637 and 638 isotopologues ordered according to the band centres. The band parameters relative to the 738 and 838 species are presented in Table 5. The *rms* values of the fits are on the order of 7×10^{-4} cm^{-1} in agreement with our experimental uncertainty. The results of the band-by-band fit of the spectroscopic parameters are given as Supplementary Material. This archive file includes for each band, the fitted spectroscopic parameters of the upper state with corresponding errors (in % and in cm^{-1}), lower state parameters of the fit fixed to the literature values and *rms* value together with the observed and calculated values of the line positions. The spectroscopic parameters of the four $^{13}C^{16}O_2$ bands obtained by Mandin [25] and Ding *et al* [6] are listed in Table 2, for comparison. For completeness, we have included in these tables, the other observed bands and transitions even when a fit of the spectroscopic parameters was not possible as a result of a too small input dataset.

It is well known that some absorption bands of carbon dioxide are affected by Coriolis or anharmonic interactions which perturb the line positions. For the few bands affected by perturbation, a Note has been added in the last column of Tables 2-4. It gives the identification of the perturber and the interaction mechanism obtained on the basis of the EH predictions. In the case of clear energy crossings leading to perturbations of a few transitions, the affected line positions were simply excluded from the input dataset used for the fit of the band parameters. In absence of energy crossing between the interacting states in the range of observed *J* values, the resulting smooth perturbations do not hamper a fit of the spectroscopic parameters (Eq. (1)) but the derived parameter values are effective and are expected to have poor extrapolation abilities.

All the observed perturbations affecting the 636 species are *intra*polyad interactions which are in general well accounted for by the EH model of Ref. [6]. Nevertheless, the perturbation affecting the 20033 state at 9159 cm^{-1}, deserves to be discussed in more details. This perturbation leads to the largest deviations compared to the EH predictions (see Fig. 4). It was identified [34] as a third order anharmonic resonance interaction of the type (ΔV_1 =3, ΔV_3 = -2) with the 50011 state near 9145 cm^{-1}. The 20033 upper state, presently observed through the

20033-10002 hot band at 7893 cm^{-1}, was indeed previously detected by ICLAS-VeCSEL as upper state of the 20033-00001 cold band [34]. The energy levels crossing at J=51 could not be observed in Ref. [34] as only transitions with maximum J values of 43 were detected. The resonance interaction responsible for the perturbation is already included in the EH model of $^{13}C^{16}O_2$ but the corresponding interaction parameter could not be accurately determined due to the lack of experimental information about the levels of the 20033 state close to the energy crossing. This is why the deviations of the observed energy level compared to the EH predictions are limited to 5.8×10^{-2} cm^{-1} while the deviations from the unperturbed energy values (Eq. (1)) reach a maximum value of 0.51 cm^{-1} around the energy crossing. We present in Fig. 5 the difference of the energy levels values of the 20033 and 50011 interacting states with the unperturbed energy values of the 20033 state calculated with the single band parameters included in Table 2. It is interesting to see that, while the transitions of the 50011-10002 band are intrinsically extremely weak (which limits the observations to J values smaller than 25), the intensity transfer induced by the coupling with the 20033 state allows observing the P and R lines of the 50011-10002 band reaching the J=47 and 49 levels.

The *intra*polyad interactions are generally very well accounted for by the EH models but our recent CRDS investigations have evidenced five occurrences of *inter*polyad interactions affecting exclusively the non symmetric isotopologues. Two occurrences were identified in the spectrum of the 628 isotopologue [23] while in the case of the ^{13}C isotopologues, three occurrences were found: 40014 (P= 11) ↔ 60007 (P= 12) in 638 [10] and 31113 (P= 10) ↔ 51106 (P= 11) in both 638 and 637 [8, 10]. These *inter*polyad interactions - all of anharmonic type - are not included in the current EH models which are polyad models. The 40014 (P= 11) ↔ 60007 (P= 12) interpolyad coupling in 638 was evidenced from the analysis of the 40014-10002 hot band at 5976 cm^{-1} [30]. It is confirmed by the present observation of the 40014-00001 cold band at 7221 cm^{-1} and the observation of two extra lines of the 60007-00001 band around the energy crossing at J= 38 (see Fig. 6). The same *inter*polyad coupling is expected to affect the $^{16}O^{13}C^{17}O$ isotopologue but the EH model of Ref. [8] predicts an energy crossing at J=45 while we observe a clear local perturbation around J=20 (see Fig. 6). The lack of experimental data used to refine the EH parameters of 637 is probably responsible for the poor quality of the predicted energy levels of the 60007 state.

V. CONCLUSION

The knowledge of the absorption spectrum of the ^{13}C isotopologues of carbon dioxide in the 1.26-1.44 μm region has been considerably improved by CW-CRDS. While about one hundred transitions were previously reported by FTS in the investigated region, more than 3800 transitions belonging to five ^{13}C isotopologues were measured by CRDS. For the 636 species for instance, 2382 transitions were detected. If we add the 4441 transitions measured by CRDS in the 5957–6833 cm^{-1} region [10], it leads to a total number of about 6700 CRDS observations for the $^{13}C^{16}O_2$ species in the whole 5957-7917 cm^{-1} region. This number represents more than half of the number of about 13000 $^{13}C^{16}O_2$ transitions obtained from an exhaustive review of the literature for the whole 0-14000 cm^{-1} region. The new observations will be valuable for refining the sets of effective Hamiltonian parameters used to generate the CDSD database. The measurements and modelling of the absorption of the considered minor isotopologues may be of importance for the analysis of the Venus spectrum in the CO_2 transparency windows.

The existence of interpolyad interactions affecting the non-symmetric isotopologues has been confirmed by the observation of the 40014 (P= 11)↔60007 (P= 12) anharmonic interaction in both $^{16}O^{13}C^{17}O$ and $^{16}O^{13}C^{18}O$. The observed up to now interpolyad resonance interactions for carbon dioxide can take place only in the case of non-symmetric isotopologues because the principal interaction matrix element in all observed cases is the $\langle V_1 V_2 \ell_2 V_3 J | H^{eff} | V_1 + 2\ V_2\ \ell_2 V_3 - 1\ J \rangle$ Fermi-type matrix element which is strictly equal to zero for symmetric isotopologues. To take into account these resonance interactions it is necessary to use a nonpolyad model of effective Hamiltonian. The solution of the Schrödinger equation will require the diagonalization of very large matrixes. Although the fitting of EH parameters is more time-consuming and the cases of interpolyad perturbations are very seldom, we plan to use nonpolyad models for the non-symmetric isotopologues in the future.

During the spectrum analysis, we noted a number of important deviations between the line intensities calculated within the effective operators approach and the observations. Following the same approach as for natural carbon dioxide [24], we will undertake line intensity retrieval from the recorded spectra in order to improve the quality of the intensity modelling in the considered region. Indeed, the only previous intensity measurements in the region are relative to the strongest transitions of the 40012-00001 and 40013-00001 bands of $^{13}C^{16}O_2$ [27] and the refinement of the dipole momentum parameters will benefit from the considerable extension of the input dataset of

line intensities. In particular, it will be possible to determine the $\Delta P = 10$ dipole parameters of the $^{16}O^{13}C^{18}O$ isotopologue which are so far unknown.

ACKNOWLEDGMENTS

This work is jointly supported by CNRS (France), RFBR (Russia) and CAS (China) in the frame of Groupement de Recherche International SAMIA (Spectroscopie des Molécules d'Intérêt Atmosphérique). We thank S.A. Tashkun for providing us with the predicted 838 line positions.

References

[1] Villanueva GL, Mumma MJ, Novak RE, Hewagama T. Discovery of multiple bands of isotopic CO_2 in the prime spectral regions used when searching for CH_4 and HDO on Mars. JQSRT 2008;109:883-94.

[2] Villanueva GL, Mumma MJ, Novak RE, Hewagama T. Identification of a new band system of isotopic CO_2 near 3.3 μm: Implications for remote sensing of biomarker gases on Mars. Icarus 2008;195:34-44.

[3] Wilquet V, Mahieux A, Vandaele AC, Perevalov VI, Tashkun SA, Fedorova A, Korablev O, Montmessin F, Dahoo R, Bertaux JL. Line parameters for the 01111–00001 band of $^{12}C^{16}O^{18}O$ from SOIR measurements of the Venus atmosphere. JQSRT 2008;109:895-905.

[4] Bertaux JL, Vandaele AC, Wilquet V, Montmessin F, Dahoo R, Villard E, Korablev O, Fedorova A. First observation of 628 CO_2 isotopologue band at 3.3 μm in the atmosphere of Venus by solar occultation from Venus Express. Icarus 2008;195:28-33.

[5] Majcherova Z, Macko P, Romanini D, Perevalov VI, Tashkun SA, Teffo JL, Campargue A. High-sensitivity CW-cavity ringdown spectroscopy of $^{12}CO_2$ near 1.5 μm. J Mol Spectrosc 2005;230:1-21.

[6] Ding Y, Macko P, Romanini D, Perevalov VI, Tashkun SA, Teffo JL, Hu SM, Campargue A. High sensitivity cw-cavity ringdown and Fourier transform absorption spectroscopies of $^{13}CO_2$. J Mol Spectrosc 2004;226:146-160.

[7] Perevalov BV, Kassi S, Romanini D, Perevalov VI, Tashkun SA, Campargue A. CW-cavity ringdown spectroscopy of carbon dioxide isotopologues near 1.5 μm. J Mol Spectrosc 2006;238:241-255.

[8] Perevalov BV, Kassi S, Romanini D, Perevalov VI, Tashkun SA, Campargue A. Global effective Hamiltonians of $^{16}O^{13}C^{17}O$ and $^{16}O^{13}C^{18}O$ improved from CW-CRDS observations in the 5900–7000 cm^{-1} region. J Mol Spectrosc 2007;241:90-100.

[9] Perevalov BV, Deleporte T, Liu AW, Kassi S, Campargue A, Vander Auwera J, Tashkun SA, and Perevalov VI. Global modeling of $^{13}C^{16}O_2$ absolute line intensities from CW-CRDS and FTS measurements in the 1.6 and 2.0 micrometer regions. JQSRT 2008;109:2009-26.

[10] Perevalov BV, Perevalov VI, Campargue A., A (nearly) complete experimental linelist for $^{13}C^{16}O_2$, $^{16}O^{13}C^{18}O$, $^{16}O\ ^{13}C^{17}O$, $^{13}C_2{}^{18}O$ and $^{17}O\ ^{13}C^{18}O$ by high sensitivity CW-CRDS spectroscopy between 5851 and 7045 cm^{-1} JQSRT 2008;109:2437-62.

[11] Perevalov BV, Kassi S, Perevalov VI, Tashkun SA, Campargue A. High sensitivity CW-CRDS spectroscopy of $^{12}C^{16}O_2$, $^{16}O^{12}C^{17}O$ and $^{16}O^{12}C^{18}O$ between 5851 and 7045 cm^{-1}: Line positions analysis and critical review of the current databases. J Mol Spectrosc 2008;252:143-59.

[12] Perevalov BV, Campargue A, Gao B, Kassi S, Tashkun SA, Perevalov VI. New CW-CRDS measurements and global modeling of $^{12}C^{16}O_2$ absolute line intensities in the 1.6 μm region. J Mol Spectrosc 2008;252:190-7.

[13] Rothman LS, Gordon IE, Barbe A, Benner DC, Bernath PF, Birk M et al. The HITRAN 2008 Molecular Spectroscopic Database. JQSRT 2009;110:533–72.

[14] Miller CE, Brown LR. Near infrared spectroscopy of carbon dioxide I. $^{16}O^{12}C^{16}O$ line positions. J Mol Spectrosc 2004;228:329-54.

[15] Toth RA, Brown LR, Miller CE, Devi VM, Benner DC. Line strengths of $^{12}C^{16}O_2$: 4550-7000 cm^{-1}. J Mol Spectrosc 2006;239:229-42.

[16] Miller CE, Montgomery MA, Onorato RM, Johnstone C, McNicholas TP, Kovaric B, Brown LR. Near infrared spectroscopy of carbon dioxide. II $^{16}O^{13}C^{16}O$ and $^{16}O^{13}C^{18}O$ line positions. J Mol Spectrosc 2004;228:355-74.

[17] Toth RA, LR Brown, Miller CE, Devi VM, Benner DC. Self-broadened widths and shifts of $^{12}C^{16}O_2$: 4550-7000 cm^{-1}. J Mol Spectrosc 2006;239:243-71.

[18] Toth RA, Miller CE, Brown LR, Devi VM, Benner DC. Line positions and strengths of $^{16}O^{12}C^{18}O$, $^{18}O^{12}C^{18}O$ and $^{17}O^{12}C^{18}O$ between 2200 and 7000 cm^{-1}. J Mol Spectrosc 2007;243:43-61.

[19] Toth RA, Brown LR, Miller CE, Devi VM, Benner DC. Air-broadened halfwidth and pressure shift coefficients of $^{12}C^{16}O_2$ bands: 4750-7000 cm^{-1}. J Mol Spectrosc 2007;242: 131-57.

[20] Toth RA, Miller CE, Brown LR, Devi VM, Benner DC. Line strengths of $^{16}O^{13}C^{16}O$, $^{16}O^{13}C^{18}O$, $^{16}O^{13}C^{17}O$ and $^{18}O^{13}C^{18}O$ between 2200 and 6800 cm^{-1}. J Mol Spectrosc 2008;251:64-89.

[21] Toth RA, Brown LR, Miller CE, Devi VM, Benner DC. Spectroscopic database of CO_2 line parameters: 4300 - 7000 cm^{-1}. JQSRT 2008;109:906-21.

[22] Perevalov VI, Tashkun SA. CDSD-296 (Carbon Dioxide Spectroscopic Databank): Updated and Enlarged Version for Atmospheric Applications. 10th HITRAN Database Conference, Cambridge MA, USA, 2008. ftp://ftp.iao.ru/pub/CDSD-2008/

[23] Kassi S, Song KF, Campargue A. High sensitivity CW-cavity ring down spectroscopy of $^{12}CO_2$ near 1.35 μm (I): line positions. JQSRT 2009;110:1801-14.

[24] Song KF, Kassi S, Tashkun SA, Perevalov VI, Campargue A. High Sensitivity *CW*-Cavity Ring Down Spectroscopy of $^{12}CO_2$ near 1.35 μm (II): New observations and Line intensities modeling. JQSRT, doi:10.1016/j.jqsrt.2009.09.004 .

[25] Mandin JY. Interpretation of the CO_2 absorption bands observed in the Venus infrared spectrum between 1 and 2.5 μm. J Mol Spectrosc 1977;67:304-21.

[26] Tashkun SA, Perevalov VI, Teffo JL, Rothman LS, Tyuterev VG. Global fitting of $^{12}C^{16}O_2$ vibrational-rotational line positions using the effective Hamiltonian approach. JQSRT 1998;60:785-801.

[27] Wang L, Perevalov VI, Tashkun SA, Ding Y, Hu SM. Absolute line intensities of $^{13}C^{16}O_2$ in the 4200–8500 cm^{-1} region. J Mol Spectrosc 2005;234:84-92.

[28] Morville J, Romanini D, Kachanov AA, Chenevier M. Two schemes for trace detection using cavity ringdown spectroscopy. Appl Phys 2004;D78:465-76.

[29] Macko P, Romanini D, Mikhailenko SN, Naumenko OV, Kassi S, Jenouvrier A, Tyuterev VG. High sensitivity CW-cavity ring down spectroscopy of water in the region of the 1.5 μm atmospheric window. J Mol Spectrosc 2004;227:90-108.

[30] Chedin A, Teffo JL. The carbon dioxide molecule: a new derivation of the potential, spectroscopic, and molecular constants. J Mol Spectrosc 1984;107:333–42.

[31] Chedin A. The carbon dioxide molecule. Potential, spectroscopic and molecular constants from its infrared spectrum. J Mol Spectrosc 1979;76:430–91.

[32] Rothman LS, Hawkins RL, Wattson RB, Gamache RR. Energy levels, intensities, and linewidths of atmospheric carbon dioxide bands. JQSRT 1992;48:537–66.

[33] Teffo JL, Claveau C, Valentin A. Infrared fundamental bands of $O^{13}C^{17}O$ isotopic variants of carbon dioxide. JQSRT 1998;59:151-64.

[34] Ding Y, Campargue A, Bertseva E, Tashkun SA, Perevalov VI. Highly sensitive absorption spectroscopy of carbon dioxide by ICLAS-VeCSEL between 8800 and 9530 cm^{-1}. J Mol Spectrosc 2005;231:117-23.

Table Captions

Table 1. Number of transitions assigned to the ^{13}C isotopologues of carbon dioxide in the CW-CRDS spectrum between 7029 and 7917 cm^{-1} and comparison with previous observations.

Table 2. Spectroscopic parameters (in cm^{-1}) of the $^{13}C^{16}O_2$ bands obtained from the analysis of the CW-CRDS spectrum in the 7029-7795 cm^{-1} region. The spectroscopic parameters of the lower states were taken from Refs. [16, 32].

Table 3. Spectroscopic parameters (in cm^{-1}) of the $^{16}O^{13}C^{18}O$ bands obtained from the analysis of the CW-CRDS spectrum in the 7029 -7795 cm^{-1} region. The spectroscopic parameters of the lower states were taken from Ref. [16].

Table 4. Spectroscopic parameters (in cm^{-1}) of the $^{16}O^{13}C^{17}O$ bands obtained from the analysis of the CW-CRDS spectrum in the 7029-7795 cm^{-1} region. The spectroscopic parameters of the ground state were taken from Ref. [32].

Table 5. Spectroscopic parameters (in cm^{-1}) of the $^{18}O^{13}C^{18}O$ and $^{18}O^{13}C^{17}O$ bands obtained from the analysis of the CW-CRDS spectrum in the 7029-7795 cm^{-1} region. The spectroscopic parameters of the ground state for $^{18}O^{13}C^{18}O$ were taken from Ref. [20] and those for $^{17}O^{13}C^{18}O$ from Ref. [33].

Figure Captions

Figure 1.
The CW-CRDS spectrum of ^{13}C enriched carbon dioxide in the region of the 40012-00001 band of $^{13}C^{16}O_2$ (P=10.0 Torr). Four successive enlargements illustrate the high sensitivity and high dynamics of the recordings: absorption coefficients differing by more than four orders of magnitude (from 4×10^{-6} cm^{-1} to the noise level at 3.1×10^{-10} cm^{-1}) can be measured from the displayed spectrum.

Figure 2:
Section of the CW-CRDS spectrum of ^{13}C enriched carbon dioxide showing the contributions of four ^{13}C isotopologues: $^{13}C^{16}O_2$, $^{16}O^{13}C^{18}O$, $^{16}O^{13}C^{17}O$ and $^{17}O^{13}C^{18}O$ (labelled 636, 638, 637, 838 and 738, respectively).

Upper panel: CW-CRDS spectrum recorded with a pressure of 10.0 Torr.

Lower panel: Spectrum predicted by the effective operators models. The line intensities were calculated assuming the same isotopic composition as in Ref. [9]. Note the important deviation between the observed and predicted positions of the 637 transition.

Figure 3.
Overview comparison of the absorption spectrum of $^{13}C^{16}O_2$, $^{16}O^{13}C^{18}O$ and $^{16}O^{13}C^{17}O$ isotopologues between 7080 -7950 cm^{-1}.

Left hand: Observed spectra: line positions are experimental values while line intensities are calculated values obtained as described in the body of the text assuming the same isotopic composition as in Ref. [9]. The $^{13}C^{16}O_2$ transitions highlighted on the upper panel correspond to the previous observations available in the literature [6, 25].

Right hand: Spectra calculated by effective operators models.

Note that the 20022-00001 and 20021-00001 bands of the $^{16}O^{13}C^{18}O$ isotopologue which belong to the ΔP= 10 series of transitions are not displayed because the corresponding ΔP= 10 effective dipole momentum parameters are not available.

Figure 4
Residuals between the measured line positions and those calculated using the EH models for $^{13}C^{16}O_2$ (636), $^{16}O^{13}C^{18}O$ (638) and $^{16}O^{13}C^{17}O$ (637) isotopologues. The largest deviations observed in 636 and 638 are due to local perturbations (see Text).

Figure 5.
Reduced energy plot relative to the anharmonic resonance interaction between the 50011 and 20033 vibrational states of $^{16}O^{13}C^{16}O$, observed through the 50011-10002 and 20033-10002 hot bands. For both 50011 and 20033 states, the energy differences between the experimental values and the unperturbed values of the 20033 state (Eq. (1)) are plotted. For each J value, the energy level obtained from the R(J -1) and P(J +1) transitions are shown (open squares and full circles, respectively). The transitions of the 50011-10002 band are extremely weak and observations are limited to J values up to 25 only. Around the energy crossing at J=51, the intensity transfer induced by the coupling with the 20033 state allows the observation of a few extra lines of the 50011-10002 band.

Figure 6.

Reduced energy plot relative to the *inter*polyad anharmonic resonance interaction between the 40014 (P= 11) ↔ 60007 (P= 12) observed through the 40014-00001 band. The energy differences are relative to the unperturbed energy values of the 40014 calculated with the fitted spectroscopic parameters listed in Table 3 for 638 and Table 4 for 637. For each J value, the energy level was obtained from the R(J -1) and P(J +1) transitions (open squares and full circles, respectively).

Upper panel: $^{16}O^{13}C^{18}O$. The J= 36 energy level of the 60007 state (×) was determined from the R(35) and P(37) extra lines.

Lower panel: $^{16}O^{13}C^{17}O$. The energy crossing is observed at J= 21.

Table 1

Number of transitions assigned to the ^{13}C isotopologues of carbon dioxide in the CW-CRDS spectrum between 7029 and 7917 cm^{-1} and comparison with previous observations.

	Number of transitions		Number of bands	
	Venus[25]/FTS[6]	**CRDS**	**Venus[25]/FTS[6]**	**CRDS**
$^{13}C^{16}O_2$ (636)	64/114	2382	4/4	56
$^{16}O^{13}C^{17}O$ (637)	0	333	0	6
$^{16}O^{13}C^{18}O$ (638)	0	1044	0	18
$^{17}O^{13}C^{18}O$ (738)	0	30	0	1
$^{18}O^{13}C^{18}O$ (838)	0	52	0	2
Total	**64/114**	**3841**	**4/4**	**83**

Table 2. Spectroscopic parameters (in cm^{-1}) of the $^{13}C^{16}O_2$ bands obtained from the analysis of the CW-CRDS spectrum in the 7029-7795 cm^{-1} region. The spectroscopic parameters of the lower states were taken from Refs. [16, 32]. When available, the values of the previous determinations of the spectroscopic parameters are given in italics.

P'-P"	**Band**	ΔG_v	G_v	B_v	$D_v \times 10^7$	$H_v \times 10^{12}$	*rms* $\times 10^3$	N_{FIT}/N_{TOT}	J_{MAX} P/Q/R	***Notes***
12-1	41115e-01101e	7088.92949(90)	7737.40785(90)	0.3893194(41)	2.015(36)		0.76	9/10	12/ /32	
12-1	41115f-01101f							/ 5	11/ /29	
11-0	40015e-00001e	7142.16022(18)	7142.16022(18)	0.39010124(86)	3.7510(89)	12.66(23)	0.48	37/37	39/ /51	
11-0	51104e-00001e	7150.4011(11)	7150.4011(11)	0.3892609(27)	0.944(15)		0.85	19/24	37/ /51	Perturbed band. 51104↔40015 Coriolis resonance interaction.
14-3	51115e-11102e							/ 3	18/ /14	
14-3	51115f-11102f							/ 6	15/ /23	
13-2	42214e-02201e	7255.16321(45)	8552.42818(45)	0.3897753(28)	2.077(41)	14.0(16)	0.75	23/24	41/ /35	
13-2	42214e-02201f							/ 1	/ 3/	
13-2	42214f-02201f	7255.16317(33)	8552.42814(33)	0.3897777(15)	1.537(12)		0.69	24/27	34/ /34	
13-2	50015e-10002e	7263.84420(26)	8529.67203(26)	0.3885944(15)	3.443(20)	11.19(65)	0.65	35/37	45/ /45	
12-1	41114e-01101e	7290.62990(15)	7939.10826(15)	0.38783370(53)	1.7789(44)	0.787(95)	0.44	49/49	56/ /56	
12-1	41114e-01101f							/ 3	/ 8/	
12-1	41114f-01101e							/ 2	/ 7/	
12-1	41114f-01101f	7290.63012(18)	7939.10848(18)	0.38973138(33)	1.9500(11)		0.58	44/44	55/ /57	
11-0	51103e-00001e	7316.63130(59)	7316.63130(59)	0.38794291(92)	1.4043(29)		0.71	18/19	41/ /55	
12-1	52203e-01101e							/ 3	36/ /28	
12-1	52203f-01101f							/ 1	19/ /	
11-0	40014e-00001e	7332.205188(87)	7332.205188(87)	0.38851802(21)	2.1336(11)	2.607(16)	0.32	64/64	65/ /71	
13-2	50014e-10001e	7333.34547(30)	8703.40763(30)	0.3859310(18)	1.321(25)	-4.30(88)	0.62	26/28	43/ /43	
11-0	32213e-00001e	7359.68722(90)	7359.68722(90)	0.3889602(12)	1.2651(34)		0.81	17/17	45/ /55	
14-3	40025e-11102e							/ 4	/ /24	
14-3	51114e-11102e							/ 4	14/ / 4	
14-3	51114f-11102f	7421.80976(37)	9318.34735(37)	0.3883655(21)	1.794(21)		0.6	15/17	23/ /31	

13-2	50014e-10002e	7437.57975(18)	8703.40758(18)	0.38593546(72)	1.3878(68)	-1.85(17)	0.45	40/43	53/ /53	
14-3	51113e-11101e							/ 5	20/ /	
14-3	51113f-11101f							/ 7	27/ /31	
13-2	61103e-10002e							/ 5	19/ /33	
13-2	42213e-02201e	7448.29457(25)	8745.55953(25)	0.3883425(12)	1.757(13)	2.77(40)	0.5	32/32	41/ /47	
13-2	42213e-02201f							/ 1	/ 5/	
13-2	42213f-02201e							/ 2	/ 4/	
13-2	42213f-02201f	7448.29416(20)	8745.55913(20)	0.38835013(61)	1.3200(34)		0.54	33/34	44/ /42	
12-1	41113e-01101e	7462.90294(18)	8111.38130(18)	0.38625695(70)	1.5343(62)	2.39(15)	0.55	49/51	54/ /58	Perturbed band. 41113e↔44402e Coriolis+ℓ-type resonance interaction Energy levels crossing at *J*=60
12-1	41113e-01101f							/ 6	/20/	
12-1	41113f-01101e							/ 4	/13/	
12-1	41113f-01101f	7462.90331(16)	8111.38167(16)	0.38793560(53)	1.5953(39)	1.357(77)	0.49	52/53	59/ /59	41113f↔44402f Coriolis+ℓ-type resonance interaction Energy levels crossing at *J*=71
13-2	50013e-10001e	7465.50103(20)	8835.56319(20)	0.38493096(83)	1.2403(76)	3.04(18)	0.6	38/38	55/ /51	
11-0	40013e-00001e	7481.57368(46)	7481.57368(46)	0.3852956(44)	-1.503(78)	-71.3(37)	0.95	22/50	71/ /75	Perturbed band. 40013↔51102e Coriolis resonance interaction. No energy levels crossing
11-0	*40013e-00001e*	*7481.57400(37)*	*7481.57400(37)*	*0.3852885(33)*	*-1.6882(66)*	*-82.6(36)*	*0.92*	*35/45*	*44/ /46*	*Ding et al [6]*
11-0	*40013e-00001e*	*7481.5700(25)*	*7481.5700(25)*	*0.38539(88)*	*1.444(56)*		*6.54*		*35/ /41*	*Mandin [25]*
11-0	51102e-00001e	7486.77606(48)	7486.77606(48)	0.3891737(30)	4.069(47)	63.0(20)	0.85	35/61	63/ /65	Perturbed band. 40013↔51102e Coriolis resonance interaction. No energy levels crossing.
11-0	32212e-00001e	7540.5229(42)	7540.5229(42)	0.3879677(80)	1.395(36)		0.79	12/14	37/ /47	
11-0	21123e-00001e	7563.30063(19)	7563.30063(19)	0.38583095(62)	1.5624(32)		0.45	20/22	45/ /15	
11-0	21123f-00001e	7563.30065(34)	7563.30065(34)	0.3872814(15)	1.719(12)		0.67	18/20	/40/	
13-2	50013e-10002e	7569.73554(19)	8835.56337(19)	0.3849277(11)	1.192(14)	1.61(48)	0.53	42/42	45/ /41	
13-2	50012e-10001e	7599.99342(26)	8970.05558(26)	0.3864641(16)	0.596(25)	2.5(10)	0.6	34/34	41/ /39	
11-0	40012e-00001e	7600.12116(11)	7600.12116(11)	0.38587898(24)	0.8431(12)	1.041(17)	0.41	70/70	67/ /73	
11-0	*40012e-00001e*	*7600.12116(19)*	*7600.12116(19)*	*0.38587618(48)*	*0.8072(22)*		*0.67*	*46/48*	*46/ /48*	*Ding et al [6]*
11-0	*40012e-00001e*	*7600.1267(4)*	*7600.1267(4)*	*0.3858775(12)*	*0.533(3)*		*1.00*		*31/ /43*	*Mandin [25]*
12-1	41112e-01101e	7619.13028(15)	8267.60864(15)	0.38606484(54)	1.0780(45)	0.707(97)	0.47	55/55	56/ /56	

12-1	41112e-01101f							/ 6	/14/	
12-1	41112f-01101e							/ 4	/15/	
12-1	41112f-01101f	7619.13024(15)	8267.60860(15)	0.38765178(48)	1.0415(36)	0.708(73)	0.45	55/56	55/ /59	
13-2	42212e-02201e	7631.31875(41)	8928.58372(41)	0.3884393(23)	3.399(33)	43.6(13)	0.67	31/33	33/ /41	
13-2	42212f-02201f	7631.31569(39)	8928.58066(39)	0.3884718(24)	2.542(37)	35.1(15)	0.71	31/32	36/ /40	
12-1	30023e-01101e	7668.68551(57)	8317.16387(57)	0.3848357(14)	1.7475(66)		0.66	14/15	/ /44	
12-1	30023e-01101f	7668.68677(86)	8317.16513(86)	0.3848344(53)	1.753(63)		0.9	9/ 9	/28/	
11-0	51101e-00001e	7682.38905(43)	7682.38905(43)	0.3887549(16)	1.042(15)	3.87(38)	0.62	30/31	37/ /51	
12-1	22222e-01101e	7702.07398(36)	8350.55235(36)	0.3856759(14)	1.2715(98)		0.69	19/19	12/ /38	
12-1	22222e-01101f	7702.07300(33)	8350.55136(33)	0.3856801(15)	1.314(14)		0.54	14/15	/36/	
12-1	22222f-01101e	7702.07288(52)	8350.55124(52)	0.3856765(21)	1.421(15)		0.82	15/19	/41/	
12-1	22222f-01101f	7702.07377(32)	8350.55214(32)	0.3856750(10)	1.4156(57)		0.72	20/20	7/ /43	
11-0	32211e-00001e	7720.0785(61)	7720.0785(61)	0.388270(18)	5.41(12)		0.97	7/21	39/ /55	Perturbed band. 21122e↔32211e Coriolis resonance interaction. Energy levels crossing at *J*=41.
11-0	32211f-00001e							/10	/52/	Perturbed band. 21122f↔32211f Coriolis resonance interaction. Energy levels crossing at *J*=48.
11-0	21122e-00001e	7726.95419(36)	7726.95419(36)	0.3844180(31)	-0.839(48)		0.77	23/48	33/ /63	Perturbed band. 21122e↔32211e Coriolis resonance interaction. Energy levels crossing at *J*=41.
11-0	21122f-00001e							/26	/54/	Perturbed band. 21122f↔32211f Coriolis resonance interaction. Energy levels crossing at *J*=48.
11-0	40011e-00001e	7749.08283(17)	7749.08283(17)	0.38756594(41)	0.6308(22)	1.282(31)	0.64	65/66	61/ /71	
12-1	60001e-01101e							/ 5	/ /40	
13-2	50011e-10001e	7774.97050(25)	9145.03266(25)	0.3884919(11)	0.6270(73)		0.68	30/31	39/ /37	
13-2	20033e-10001e	7788.80800(37)	9158.87016(37)	0.3832140(16)	1.808(13)		0.76	23/26	33/ /35	
12-1	41111e-01101e	7790.70988(26)	8439.18824(26)	0.3850267(74)	29.39(51)	1743.(96)	0.31	17/50	48/ /54	Perturbed band. 41111e↔30022 Coriolis resonance interaction. Energy levels crossing at *J*=20. A few *R* lines observed. The values of the parameters should be considered as effective. .
12-1	41111e-01101f							/ 4	/ 8/	

12-1	41111f-01101e							/ 5	/ 9/	
12-1	41111f-01101f	7790.71015(18)	8439.18851(18)	0.38871551(38)	0.7458(15)		0.64	50/52	51/ /55	
12-1	30022e-01101e							/34	42/ /42	Perturbed band. 41111e↔30022 Coriolis resonance interaction. Energy levels crossing at *J*=20
12-1	30022e-01101f							/ 5	/18/	
15-4	22233e-12202e							/ 3	13/ /19	
15-4	22233f-12202f							/ 2	/ /16	
15-4	30034e-20003e							/ 6	13/ /21	
13-2	42211e-02201e	7824.02112(89)	9121.28609(89)	0.3906891(87)	8.13(17)		0.91	12/27	35/ /37	Perturbed band. 42211↔61101 Coriolis resonance interaction. No energy levels crossing.
13-2	42211e-02201f							/ 1		
13-2	42211f-02201f	7824.01570(47)	9121.28067(47)	0.3908074(29)	-1.868(33)		0.86	18/25	26/ /30	
14-3	13332e-03301e	7836.56263(38)	9782.91261(38)	0.3843160(29)	1.454(54)	1.4(27)	0.61	24/29	36/ /38	
14-3	13332e-03301f							/ 4	/10/	
14-3	13332f-03301e							/ 4	/ 9/	
14-3	13332f-03301f	7836.56244(52)	9782.91242(52)	0.3843186(31)	1.541(44)	7.0(17)	0.83	29/35	41/ /41	
14-3	21133e-11102e	7849.69096(27)	9746.22854(27)	0.38303430(75)	1.5802(37)		0.8	39/41	46/ /44	
14-3	21133e-11102f							/ 1	/ 2/	
14-3	21133f-11102e							/ 2	/ 3/	
14-3	21133f-11102f	7849.69075(24)	9746.22833(24)	0.38446042(66)	1.7127(34)		0.72	36/39	47/ /39	
11-0	21121e-00001e	7867.83136(16)	7867.83136(16)	0.38397330(30)	1.08810(86)		0.6	41/41	27/ /63	
11-0	21121f-00001e	7867.83099(22)	7867.83099(22)	0.38496463(37)	1.0479(12)		0.59	28/28	/60/	
12-1	22221e-01101e	7871.04128(56)	8519.51964(56)	0.3852570(19)	1.242(12)		0.73	12/12	/ /40	
12-1	22221e-01101f	7871.04264(72)	8519.52100(72)	0.3852553(23)	1.230(15)		0.72	9/ 9	/38/	
12-1	22221f-01101e	7871.0413(10)	8519.5196(10)	0.3852657(75)	1.26(11)		0.86	8/11	/25/	
12-1	22221f-01101f	7871.04371(49)	8519.52207(49)	0.3852502(14)	1.0624(76)		0.67	10/16	/ /43	
14-3	21132e-11101e	7873.70632(41)	9910.79990(41)	0.3813599(18)	0.494(16)		0.68	18/22	34/ /22	
14-3	21132f-11101f	7873.70884(49)	9910.80242(49)	0.3826286(22)	1.184(18)		0.88	21/25	33/ /35	
13-2	50011e-10002e	7879.20394(35)	9145.03177(35)	0.3884990(14)	0.7237(68)		0.54	11/17	49/ /49	Perturbed band. 50011e↔20033 anharmonic resonance interaction. The transitions with *J'*=25-41 are not observed (see Fig.5). Energy levels crossing at *J*=50

13-2	12232e-02201e	7882.21898(24)	9179.48394(24)	0.3836435(12)	1.179(14)	8.73(43)	0.59	37/42	59/ /49	Perturbed band. 12232e↔23321e Coriolis resonance interaction.
13-2	12232e-02201f	7882.21959(52)	9179.48455(52)	0.3836395(47)	1.084(72)		0.61	8/ 9	/25/	
13-2	12232f-02201e	7882.21929(40)	9179.48426(40)	0.3836440(40)	1.483(67)		0.53	9/10	/24/	
13-2	12232f-02201f	7882.21888(24)	9179.48385(24)	0.3836435(12)	1.506(15)	10.71(47)	0.53	33/40	56/ /48	Perturbed band. 12232f↔2332Coriolis resonance interaction. Energy levels crossing at *J*=66.
14-3	10042e-00011e	7889.29277(49)	10172.77993(49)	0.3794059(16)	1.581(11)		0.75	16/20	38/ /32	
13-2	20033e-10002e	7893.04359(26)	9158.87142(26)	0.3832065(13)	1.692(14)	-4.88(29)	0.65	34/55	61/ /61	Perturbed band. 50011e↔20033 anharmonic resonance interaction. Energy levels crossing at *J*=50
12-1	30021e-01101e							/ 3	36/ / 6	
12-1	30021e-01101f							/ 8	/26/	
12-1	11132e-01101e	7929.90724(36)	8578.38560(36)	0.38243537(84)	1.4828(45)	1.169(66)	0.7	34/43	68/ /36	Data from Ref.[6] were used above 7917 cm^{-1}
12-1	*11132e-01101e*	*7929.9162(17)*		*0.3823824(203)*	*0.5(5)*		*1.47*		*18/ /18*	*Mandin [25]*
12-1	*11132e-01101e*	*7929.9100(11)*	*8578.77043(11)*	*0.3824275(42)*	*1.405(32)*		*1.52*	*23/28*	*35/ /35*	*Ding et al [6]*
12-1	11132f-01101f	7929.90786(30)	8578.38622(30)	0.38339395(65)	1.5502(32)	0.114(42)	0.78	37/50	73/ /35	Data from Ref.[6] were used above 7917 cm^{-1}
12-1	*11132f-01101f*	*7929.9050(39)*		*0.3834542(354)*	*2.60 (59)*		*4.21*		*13/ /23*	*Mandin [25]*
12-1	*11132f-01101f*	*7929.90744(72)*	*8578.76888(72)*	*0.3833988(34)*	*1.585(32)*		*1.54*	*27/31*	*32/ /34*	*Ding et al [6]*
13-2	20032e-10001e	7932.07322(75)	9302.13538(75)	0.3811466(13)	1.4958(43)		0.7	13/13	53/ /	
11-0	10032e-00001e	7981.18030(11)	7981.18030(11)	0.38227962(23)	1.5684(11)	0.273(13)	0.4	63/66	77/ /57	Data from Ref.[6] were used above 7917 cm^{-1}
11-0	*10032e-00001e*	*7981.18630(14)*		*0.3822778(4)*	*1.567(2)*		*0.50*		*43/ /47*	*Mandin [25]*
11-0	*10032e-00001e*	*7981.18048(12)*	*7981.18048(12)*	*0.38827873(23)*	*1.55786(80)*		*0.46*	*53/56*	*54/ /56*	*Ding et al [6]*

Notes.
rms: Standard deviation of the fit of the rovibrational parameters
N_{FIT}: Number of line positions included in the fit.
N_{TOTAL}: Total number of line positions assigned to the considered band.
J_{MAX}**:** Maximum value of the rotational quantum number of the upper state for the assigned transitions.

Table 3. Spectroscopic parameters (in cm^{-1}) of the $^{16}O^{13}C^{18}O$ bands obtained from the analysis of the CW-CRDS spectrum in the 7029 - 7795 cm^{-1} region. The spectroscopic parameters of the lower states were taken from Ref. [16]. When available, the values of the previous determinations of the spectroscopic parameters are given in italics.

P'-P''	Band	ΔG_v	G_v	B_v	$D_v \times 10^{-7}$	$H_v \times 10^{-12}$	rms $\times 10^{-3}$	N_{FIT}/N_{TOTAL}	J_{MAX} P/Q/R	Notes
10-0	20022e-00001e	7017.89259(31)	7017.89259(31)	0.36211415(94)	1.2547(52)		0.88	44/57	49/ /36	ΔP=10 Data from Ref.[10] were used below 7029 cm^{-1}
10-0	*20022e-00001e*	*7017.89243(41)*	*7017.89243(41)*	*0.3621140(13)*	*1.2530(72)*		*–1.28*	*45/51*	*49/ /34*	*Perevalov et al* [10]
10-0	20021e-00001e	7125.35001(17)	7125.35001(17)	0.36266470(47)	0.8418(23)		0.7	58/60	34/ /48	ΔP=10
12-1	41114e-01101e	7177.60575(45)	7820.92449(45)	0.3654524(19)	1.386(16)		0.74	24/28	33/ /39	
12-1	41114f-01101f	7177.60450(38)	7820.92324(38)	0.3671302(20)	1.618(21)		0.75	26/29	26/ /31	
12-0	60007e-00001e							/2	36/ /36	*R*(35) and *P*(37) observed only. Intensity transfer from the 40014 state due to interpolyad resonance Fermi interaction. Energy levels crossing at *J*=36 (see Fig. 6).
11-0	40014e-00001e	7220.73659(23)	7220.73659(23)	0.3658373(10)	1.9006(89)	2.65(21)	0.94	54/89	57/ /55	Perturbed band. 40014↔60007 interpolyad resonance Fermi interaction. Energy levels crossing at *J*=36 (see Fig. 6).
12-1	41113e-01101e	7339.40807(21)	7982.72681(21)	0.36450108(69)	1.1975(42)		0.69	48/50	38/ /44	
12-1	41113e-01101f							/ 1	/ 1/	
12-1	41113f-01101f	7339.40822(19)	7982.72696(19)	0.36596786(78)	1.2333(61)		0.56	45/52	36/ /45	
11-0	40013e-00001e	7351.69046(14)	7351.69046(14)	0.36375591(79)	0.406(10)	-11.95(34)	0.54	79/104	57/ /65	Perturbed band. 40013↔24412 Fermi + $\Delta\ell_2$=4 type resonance interaction. Energy levels crossing at *J*=47.
11-0	51102e-00001e	7359.97677(96)	7359.97677(96)	0.3675647(51)	1.708(72)	11.6(29)	0.88	23/29	39/ /37	
11-0	40012e-00001e	7478.62385(17)	7478.62385(17)	0.36486390(91)	0.727(11)	-14.21(35)	0.68	79/89	55/ /51	Perturbed band. 40012↔21123 Coriolis resonance interaction. Energy levels crossing at *J*=60.
11-0	21123e-00001e							/ 4	/ /46	
12-1	41112e-01101e	7500.5048(16)	8143.8236(16)	0.3648672(74)	1.012(73)		0.71	12/19	28/ /28	
12-1	41112f-01101f	7500.5018(22)	8143.8206(22)	0.366419(11)	1.07(14)		0.75	11/23	29/ /28	
11-0	40011e-00001e	7647.54288(55)	7647.54288(55)	0.3664252(20)	0.594(14)		0.73	20/22	/ /36	
11-0	21121e-00001e	7779.6349(11)	7779.6349(11)	0.3627424(52)	1.001(50)		0.82	8/13	/ /31	

11-0	21121f-00001e							/ 2	/18/	
13-2	12232e-02201e	7810.99078(40)	9097.96365(40)	0.3617600(38)	1.408(90)	13.3(59)	0.81	44/48	31/ /32	ef blended, both ef lines included in the fit
13-2	12232e-02201f							/ 1	/ 2/	
13-2	12232f-02201f	7810.99080(41)	9097.96368(41)	0.3617595(38)	1.413(90)	13.2(59)	0.83	45/49	31/ /32	ef blended, both ef lines included in the fit
13-2	20033e-10002e	7827.00230(25)	9071.90208(25)	0.36120859(85)	1.6051(54)		0.89	55/65	42/ /39	
13-2	20032e-10001e	7855.91003(54)	9198.18719(54)	0.3594108(27)	1.387(27)		0.83	21/23	28/ /31	
12-1	11132e-01101e	7859.10157(16)	8502.42031(16)	0.36065063(29)	1.3112(10)		0.75	94/96	56/ /56	
12-1	11132e-01101f							/ 5	/ 6/	
12-1	11132f-01101e							/ 6	/11/	
12-1	11132f-01101f	7859.10138(13)	8502.42013(13)	0.36149401(25)	1.38421(87)		0.61	92/98	56/ /55	
11-0	10032e-00001e	7911.56875(13)	7911.56875(13)	0.36043358(37)	1.4004(23)	0.154(36)	0.55	70/71	67/ / 8	

Notes.
rms: Standard deviation of the fit of the rovibrational parameters.
N_{FIT}: Number of line positions included in the fit.
N_{TOTAL}: Total number of line positions assigned to the considered band.
J_{MAX}**:** Maximum value of the rotational quantum number of the upper state for the assigned transitions.

Table 4. Spectroscopic parameters (in cm^{-1}) of the $^{16}O^{13}C^{17}O$ bands obtained from the analysis of the CW-CRDS spectrum in the 7029 - 7795 cm^{-1} region. The spectroscopic parameters of the ground state were taken from Ref. [32].

P'-P''	Band	ΔG_v	G_v	B_v	$D_v \times 10^{-7}$	$H_v \times 10^{-12}$	rms $\times 10^{-3}$	N_{FIT}/N_{TOTAL}	J_{MAX} P/Q/R	Notes
11-0	40014e 00001e	7274.59178(36)	7274.59178(36)	0.3765562(37)	2.203(46)	9.7(15)	0.77	28/57	42/ /43	Perturbed band. 40014↔60007 interpolyad resonance Fermi interaction. Energy levels crossing at J=20 (see Fig. 6).
11-0	40013e 00001e	7413.98240(24)	7413.98240(24)	0.3738674(17)	-0.759(26)	-40.62(82)	0.79	54/78	47/ /48	Perturbed band. 40013↔51102 Coriolis resonance interaction. No energy levels crossing.
11-0	40012e 00001e	7535.27014(16)	7535.27014(16)	0.37491417(59)	0.7367(38)		0.68	70/73	41/ /40	
11-0	40011e 00001e	7694.76051(73)	7694.76051(73)	0.3764623(44)	0.716(49)		0.76	14/23	16/ /29	
12-1	11132e 01101e	7892.47012(40)	8538.21412(40)	0.3709214(14)	1.3225(91)		0.8	23/45	40/ /37	
12-1	11132e-01101f							/ 1	/1/	
12-1	11132f 01101f	7892.46748(30)	8538.21148(30)	0.37187031(91)	1.4222(50)		0.65	32/39	42/ /42	
11-0	10032e 00001e	7943.4565(21)	7943.4565(21)	0.3704508(31)	1.071(11)		0.61	15/17	47/ /	

Notes.
rms: Standard deviation of the fit of the rovibrational parameters
N_{FIT}: Number of line positions included in the fit.
N_{TOTAL}: Total number of line positions assigned to the considered band.
J_{MAX}**:** Maximum value of the rotational quantum number of the upper state for the assigned transitions.

Table 5. Spectroscopic parameters (in cm^{-1}) of the $^{18}O^{13}C^{18}O$ and $^{18}O^{13}C^{17}O$ bands obtained from the analysis of the CW-CRDS spectrum in the 7029 -7795 cm^{-1} region. The spectroscopic parameters of the ground state for $^{18}O^{13}C^{18}O$ were taken from Ref. [20] and those for $^{17}O^{13}C^{18}O$ from Ref. [33].

Isotopologue	***P'-P"***	**Band**	ΔG_v	G_v	B_v	$D_v \times 10^{-7}$	***rms*** $\times 10^{-3}$	N_{FIT}/N_{TOTAL}	J_{MAX} P/R
$^{18}O^{13}C^{18}O$	11-0	10032e-00001e	7835.58744(17)	7835.58744(17)	0.33924858(42)	1.2333(18)	0.6	41/41	47/51
	11-0	10031e-00001e	7929.83696(90)	7929.83696(90)	0.3390166(18)	0.8867(72)	0.74	11/11	47/
$^{17}O^{13}C^{18}O$	11-0	10032e-00001e	7871.54989(49)	7871.54989(49)	0.3492844(19)	1.320(16)	0.83	25/30	34/34

Notes.
rms: Standard deviation of the fit of the rovibrational parameters
N_{FIT}: Number of line positions included in the fit.
N_{TOTAL}: Total number of line positions assigned to the considered band.
J_{MAX}**:** Maximum value of the rotational quantum number of the upper state for the assigned transitions.

Figure(s)

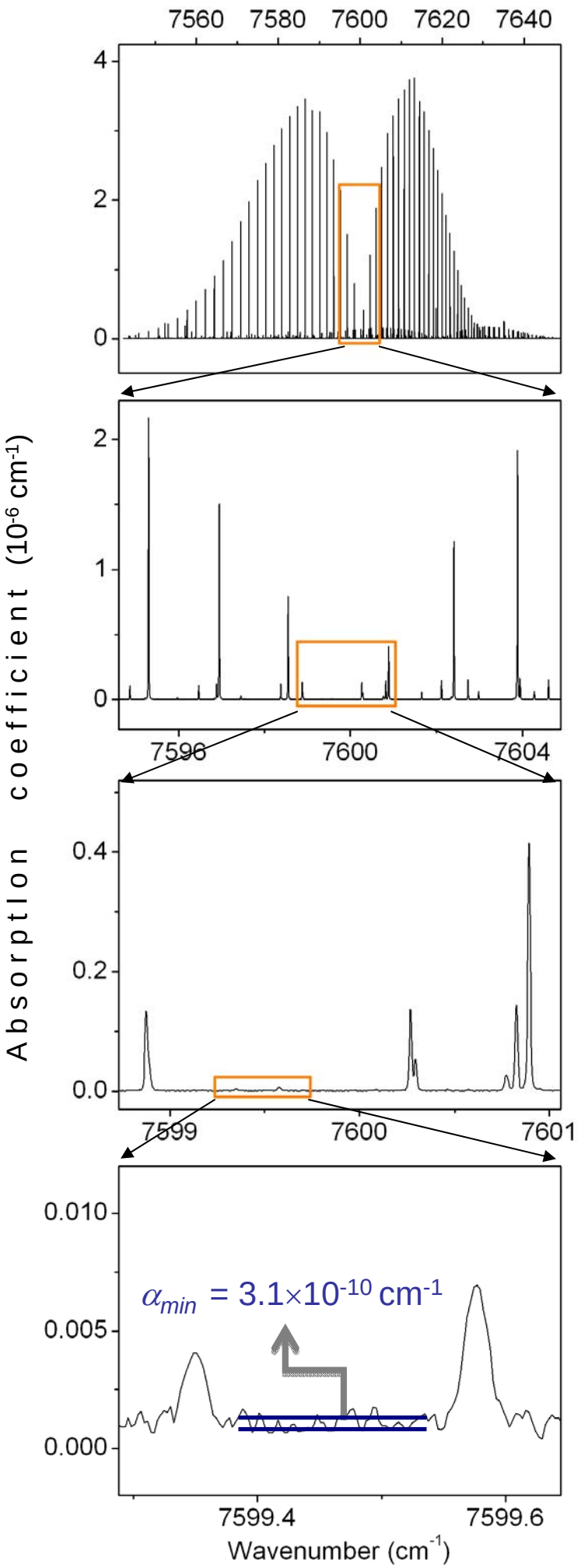
7560 7580 7600 7620 7640
4
2
0
2
1
0
7596 7600 7604
0.4
0.2
0.0
7599 7600 7601
0.010
0.005
0.000
α_{min} = 3.1×10^{-10} cm^{-1}
7599.4 7599.6
Wavenumber (cm^{-1})
Absorption coefficient (10^{-6} cm^{-1})

Fig. 2

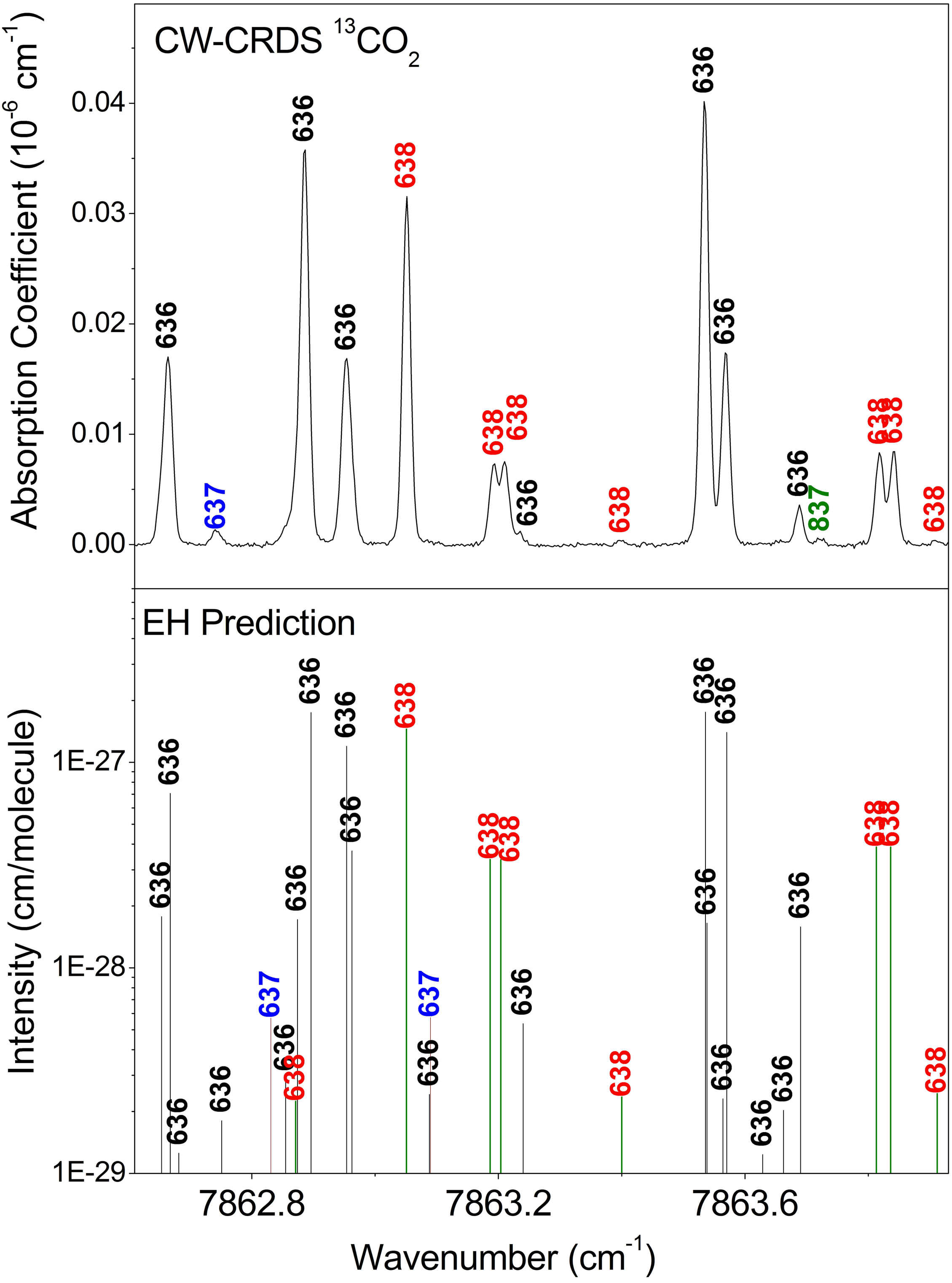
CW-CRDS $^{13}CO_2$
Absorption Coefficient (10^{-6} cm^{-1})
0.04
0.03
0.02
0.01
0.00
EH Prediction
Intensity (cm/molecule)
1E-27
1E-28
1E-29
7862.8
7863.2
7863.6
Wavenumber (cm^{-1})
636
637
638
837

Fig.3

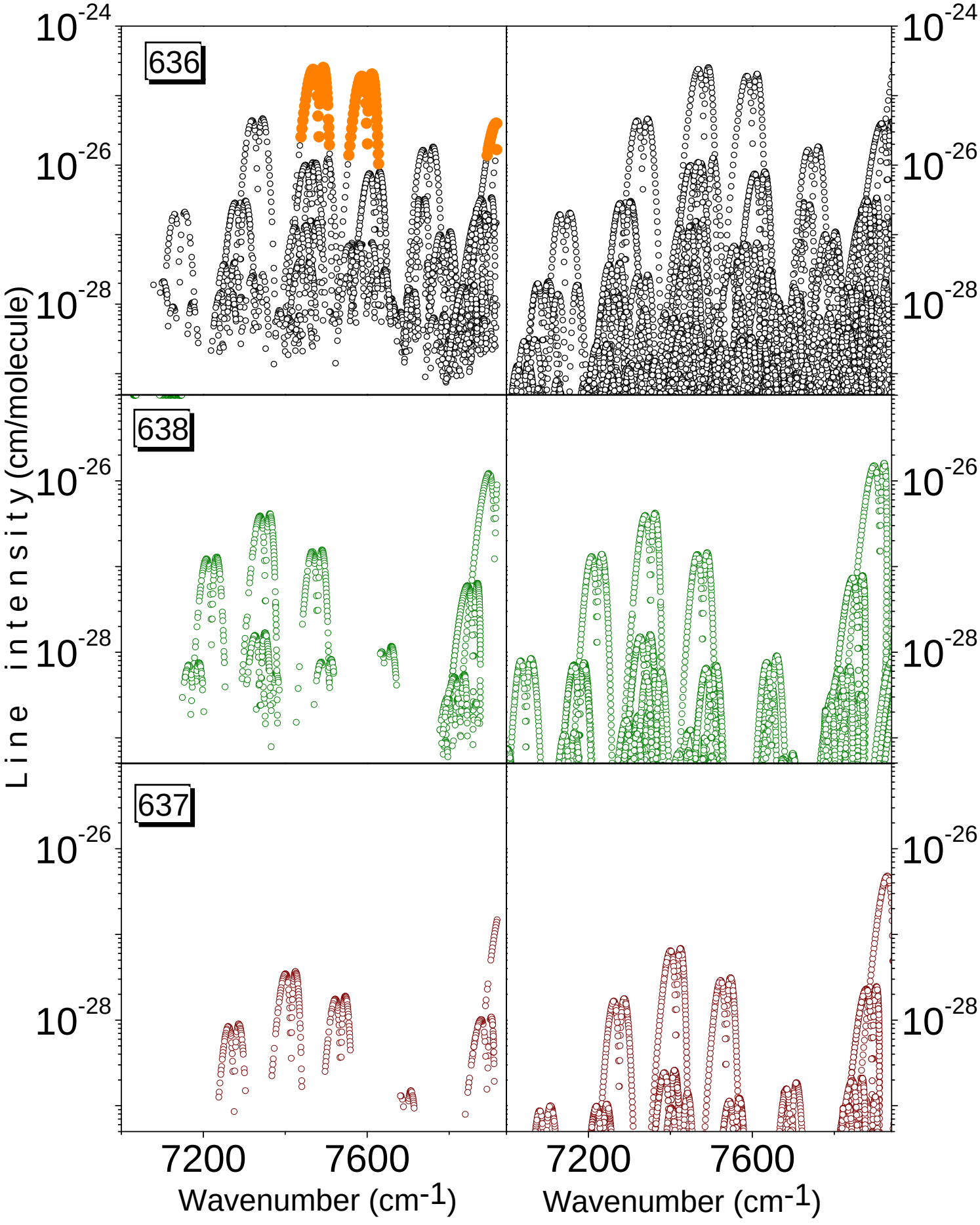
636
638
637
Line intensity (cm/molecule)
10-24
10-26
10-28
7200
7600
Wavenumber (cm-1)

Fig.4

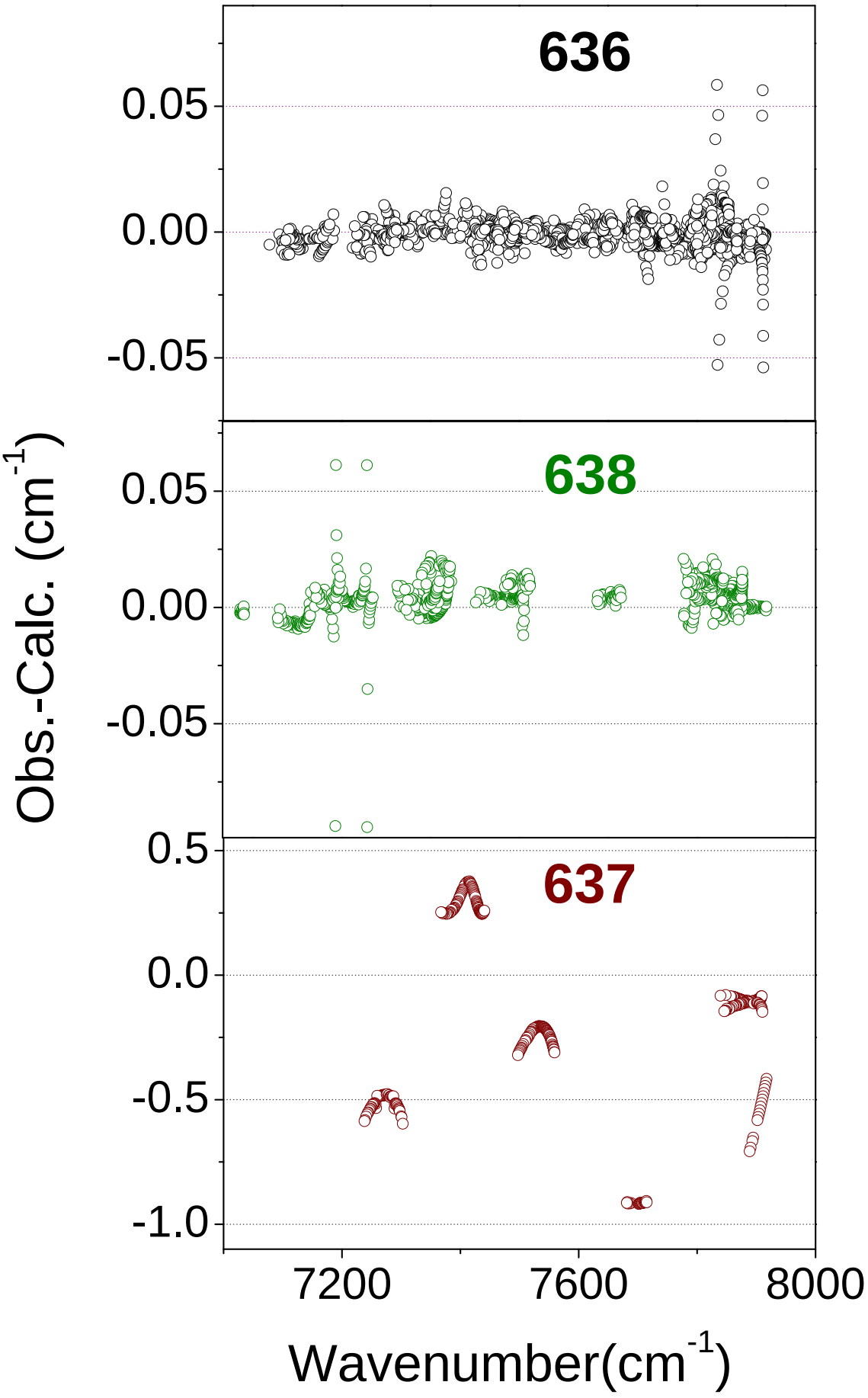
636
638
637
0.05
0.00
-0.05
0.5
0.0
-0.5
-1.0
7200
7600
8000
Obs.-Calc. (cm-1)
Wavenumber(cm-1)

Fig. 5

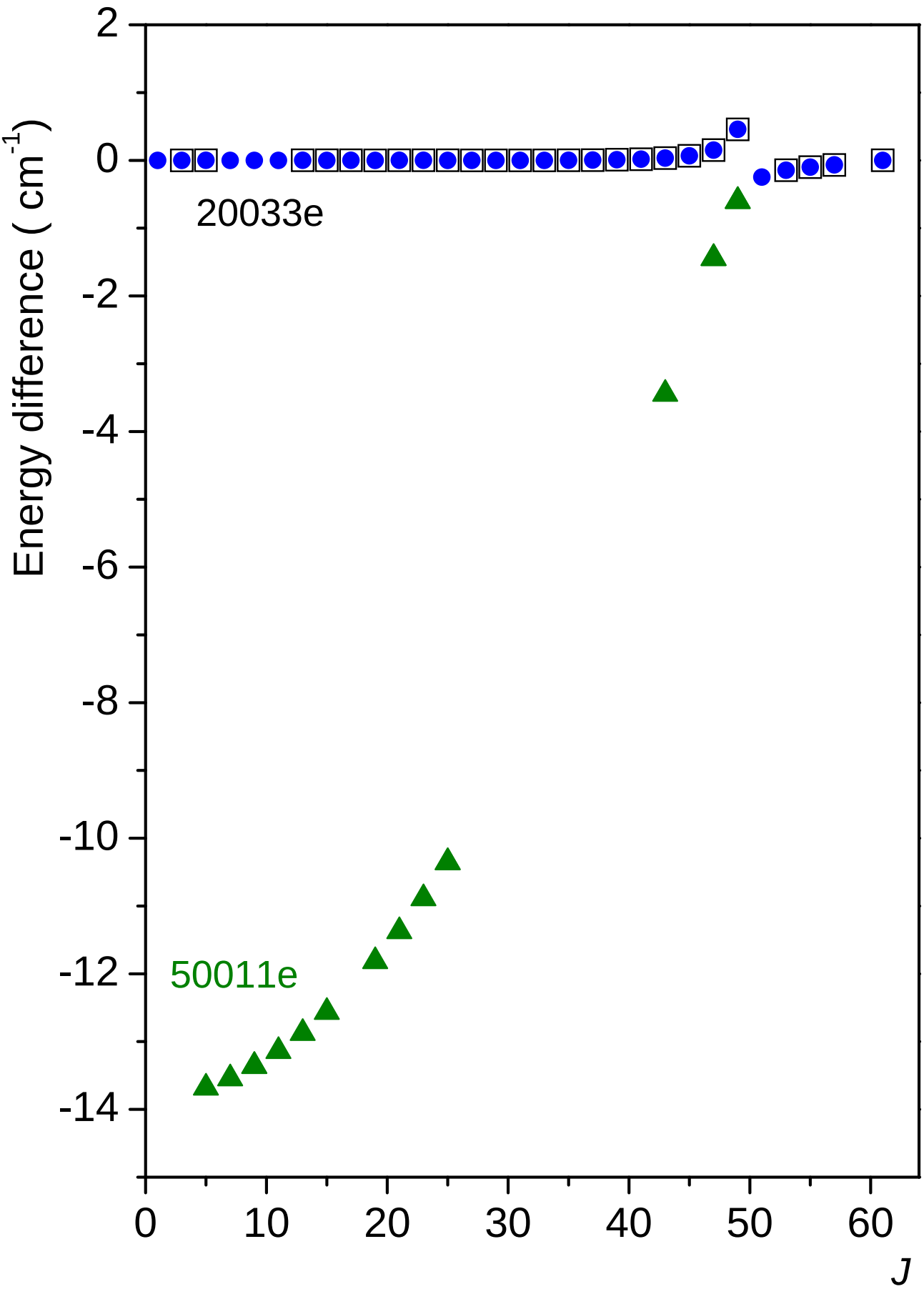
Energy difference (cm-1)
2
0
-2
-4
-6
-8
-10
-12
-14
20033e
50011e
0
10
20
30
40
50
60
J

Fig.6

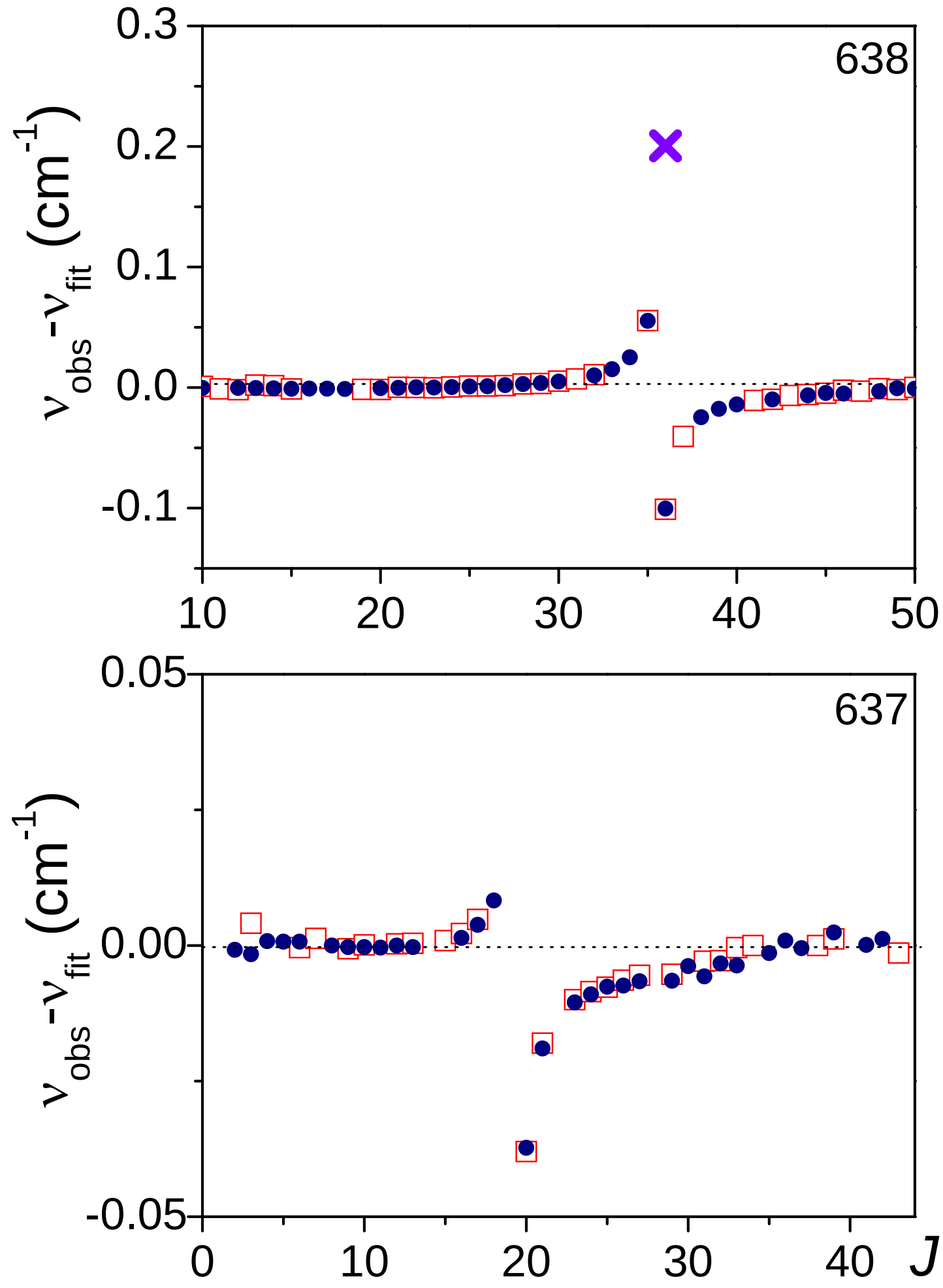
638
0.3
0.2
0.1
0.0
-0.1
10
20
30
40
50
ν_{obs}-ν_{fit} (cm^{-1})
637
0.05
0.00
-0.05
0
10
20
30
40
J
ν_{obs}-ν_{fit} (cm^{-1})

e-component, for online publication only

Click here to download e-component, for online publication only: readme.txt

e-component, for online publication only

Click here to download e-component, for online publication only: linelist_13C.txt

e-component, for online publication only

Click here to download e-component, for online publication only: 636_fit_output.txt

e-component, for online publication only

Click here to download e-component, for online publication only: 637_fit_output.txt

e-component, for online publication only

Click here to download e-component, for online publication only: 638_fit_output.txt

e-component, for online publication only

Click here to download e-component, for online publication only: 738_fit_output.txt

e-component, for online publication only

Click here to download e-component, for online publication only: 838_fit_output.txt